doi:10.1093/brain/awn328 Brain 2009: 132; 426–438 | 426

BRAIN
A JOURNAL OF NEUROLOGY

Hereditary spastic paraplegia is a novel phenotype for *GJA12/GJC2* mutations

Jennifer L. Orthmann-Murphy,[1] Ettore Salsano,[2] Charles K. Abrams,[3,4] Alberto Bizzi,[5] Graziella Uziel,[6] Mona M. Freidin,[3] Eleonora Lamantea,[7] Massimo Zeviani,[7] Steven S. Scherer[1] and Davide Pareyson[2]

1 Department of Neurology, University of Pennsylvania School of Medicine, Room 464 Stemmler Hall, 3450 Hamilton Walk, Philadelphia, PA 19104-6077, USA
2 Biochemistry and Genetics Unit, IRCCS Foundation, C. Besta Neurological Institute, Via Celoria 11, 20133 Milan, Italy
3 Department of Neurology, SUNY Downstate Medical Center, Box 1213, 450 Clarkson Avenue, Brooklyn, NY 11203, USA
4 Department of Physiology and Pharmacology, SUNY Downstate Medical Center, Box 1213, 450 Clarkson Avenue, Brooklyn, NY 11203, USA
5 Neuroradiology Unit, IRCCS Foundation, C. Besta Neurological Institute, Via Celoria 11, 20133 Milan, Italy
6 Child Neurology Unit, IRCCS Foundation, C. Besta Neurological Institute, Via Celoria 11, 20133 Milan, Italy
7 Molecular Neurogenetics Unit, IRCCS Foundation, C. Besta Neurological Institute, Via Celoria 11, 20133 Milan, Italy

Correspondence to: Davide Pareyson, MD,
Biochemistry and Genetics Unit, IRCCS Foundation,
C. Besta Neurological Institute, Via Celoria 11,
20133 Milan, Italy
E-mail: dpareys@istituto-besta.it

Recessive mutations in *GJA12/GJC2*, the gene that encodes the gap junction protein connexin47 (Cx47), cause Pelizaeus-Merzbacher-like disease (PMLD), an early onset dysmyelinating disorder of the CNS, characterized by nystagmus, psychomotor delay, progressive spasticity and cerebellar signs. Here we describe three patients from one family with a novel recessively inherited mutation, 99C>G (predicted to cause an Ile>Met amino acid substitution; I33M) that causes a milder phenotype. All three had a late-onset, slowly progressive, complicated spastic paraplegia, with normal or near-normal psychomotor development, preserved walking capability through adulthood, and no nystagmus. MRI and MR spectroscopy imaging were consistent with a hypomyelinating leukoencephalopathy. The mutant protein forms gap junction plaques at cell borders similar to wild-type (WT) Cx47 in transfected cells, but fails to form functional homotypic channels in scrape-loading and dual whole-cell patch clamp assays. I33M forms overlapping gap junction plaques and functional channels with Cx43, however, I33M/Cx43 channels open only when a large voltage difference is applied to paired cells. These channels probably do not function under physiological conditions, suggesting that Cx47/Cx43 channels between astrocytes and oligodendrocytes are disrupted, similar to the loss-of-function endoplasmic reticulum-retained Cx47 mutants that cause PMLD. Thus, *GJA12/GJC2* mutations can result in a milder phenotype than previously appreciated, but whether I33M retains a function of Cx47 not directly related to forming functional gap junction channels is not known.

Keywords: spastic paraplegias; Pelizaeus-Merzbacher-like disease; gap junction; connexin; oligodendrocyte

Abbreviations: Cx47 = connexin47; DTRs = deep tendon reflexes; ER = endoplasmic reticulum; HSP = hereditary spastic paraplegia; PMD = Pelizaeus-Merzbacher disease; PMLD = Pelizaeus-Merzbacher-like disease

Received September 16, 2008. Revised October 27, 2008. Accepted November 4, 2008. Advance Access publication December 4, 2008

Introduction

Pelizaeus-Merzbacher disease (PMD) is an X-linked disorder caused by mutations in *PLP1*, the gene encoding proteolipid protein, the main protein in CNS myelin. Classic PMD affects boys and is characterized by nystagmus and impaired psychomotor development within the first year of life, followed by progressive spasticity, ataxia, choreoathetosis and diffuse white matter changes on MRI (Nave and Boespflug-Tanguy, 1996; Hudson *et al*., 2004; Inoue, 2005). *PLP1* mutations may also cause a more severe 'connatal' PMD phenotype, which is characterized by dramatic psychomotor impairment from birth, with hypotonia, quadriplegia, nystagmus, seizures and early death. Yet other *PLP1* mutations cause a much milder disease, a 'pure' spastic paraplegia type 2 (SPG2), or a more 'complicated' form, with onset in childhood or adolescence, and dysarthria, mental retardation and ataxia (Garbern *et al*., 1999; Hudson *et al*., 2004; Garbern, 2007).

Pelizaeus-Merzbacher-like disease (PMLD) is clinically and neuroradiologically similar to classic PMD, but is not associated with *PLP1* mutations. Recessive mutations in *GJA12* are one cause of PMLD (Uhlenberg *et al*., 2004; Bugiani *et al*., 2006; Salviati *et al*., 2007; Wolf *et al*., 2007; Henneke *et al*., 2008). *GJA12/GJC2* (*GJA12* was recently renamed *GJC2*; http://www.genenames.org/genefamily/gj.php) encodes connexin47 (Cx47), which is a member of the connexin family, highly conserved integral membrane proteins usually named according to their predicted molecular mass (Willecke *et al*., 2002). Connexins form gap junctions, which are intercellular channels that form between apposed cell membranes to permit the diffusion of ions and small molecules typically less than 1000 Da (Bruzzone *et al*., 1996). Six connexins oligomerize into a hemichannel (or connexon), and two apposing hemichannels form the gap junction; aggregates of tens to thousands of intercellular channels form a gap junction plaque. The potential diversity of gap junction composition is immense, as over 20 mammalian connexins have been described. Hemichannels may be homomeric, containing one type of connexin, or heteromeric, containing more than one type. Gap junctions are termed homotypic if the apposed hemichannels contain the same connexin, and heterotypic if they contain different connexins (Kumar and Gilula, 1996).

Anatomical and functional studies of the mammalian CNS have demonstrated that astrocytes and oligodendrocytes are coupled by gap junctions, forming a 'glial syncytium' (Mugnaini, 1986; Rash *et al*., 2001; Orthmann-Murphy *et al*., 2008). There are abundant gap junctions between astrocytes (A/A), fewer between oligodendrocytes and astrocytes (O/A), and few or none between oligodendrocytes themselves. Oligodendrocytes express Cx32 and Cx47 (Dermietzel *et al*., 1989; Micevych and Abelson, 1991; Scherer *et al*., 1995; Li *et al*., 1997; Menichella *et al*., 2003; Nagy *et al*., 2003*a*; Odermatt *et al*., 2003; Kamasawa *et al*., 2005), as well as Cx29, which does not appear to form gap junctions (Altevogt *et al*., 2002; Li *et al*., 2002; Altevogt and Paul, 2004; Kleopa *et al*., 2004); cf. (Nagy *et al*., 2003*a*). Astrocytes express Cx30 and Cx43 (Dermietzel *et al*., 1989; Yamamoto *et al*., 1990; Micevych and Abelson, 1991; Nagy *et al*., 1997; Kunzelmann *et al*., 1999; Nagy *et al*., 1999, 2001, 2003*b*; Rash *et al*., 2001). A/A coupling appears to be limited to homotypic channels [Cx43/Cx43 and Cx30/Cx30; (Swenson *et al*., 1989; Werner *et al*., 1989; Dahl *et al*., 1996)], but does not include Cx30/Cx43 heterotypic channels (Orthmann-Murphy *et al*., 2007*b*). O/A coupling is most likely mediated by Cx47/Cx43 and Cx32/Cx30 heterotypic channels (Orthmann-Murphy *et al*., 2007*b*).

In humans, Cx47/Cx43 channels appear to be essential for the proper maintenance of myelin. PMLD-associated mutations are recessive and result in the loss-of-function of Cx47, including the ability to form functional channels with Cx43, suggesting that the loss of O/A coupling mediated by Cx47/Cx43 channels causes PMLD (Orthmann-Murphy *et al*., 2007*a*, *b*). Here, we describe a novel mutation (I33M) in *GJA12/GJC2* in three members of one family who have complicated hereditary spastic paraplegia (HSP). In a cell model system, the mutant protein forms gap junction plaques with Cx43, but I33M/Cx43 channels have such severely altered voltage dependent gating that they would not be predicted to function under physiological conditions.

Methods

MRI studies

MRI was performed with a 1.5 Tesla MR unit (Siemens Magnetom Avanto, Erlangen, Germany). The imaging protocol included sagittal T_1-weighted spin-echo, axial T_1-weighted inversion-recovery turbo spin-echo, axial proton-spin density and T_2-weighted turbo spin-echo and coronal FLAIR. Single-section multivoxel 2D ^{1}H MR spectroscopic imaging (^{1}H MRSI) was acquired in all patients with a PRESS technique (repetition time (T_R)/echo time (T_E) = 1200/144 ms), with a nominal planar resolution of 1.04 mm^3 (matrix = 24 × 24; field of view = 200 × 200 × 15 mm^3). The volume of interest was positioned at the level of the centrum semiovale. Scan acquisition time was 14 min. ^{1}H MRSI data were reconstructed and processed by using 'csx2' software (Soher *et al*., 1996). Imaging of the cervical spine with sagittal T_1- and T_2-weighted and axial T_2-weighted MR images was acquired for patient III-8.

Mutation analysis

Oligonucleotide primers (Uhlenberg *et al*., 2004) were used to PCR-amplify the single coding exon of *GJA12/GJC2* from genomic DNA in three overlapping fragments, which were sequenced as previously described (Bugiani *et al*., 2006).

Expression analysis of the I33M mutant

We generated the 99C>G (I33M) *GJA12/GJC2* mutation from a human Cx47 cDNA sequence (GenBank accession number AF014643) using the QuikChange kit for PCR site-directed mutagenesis (Stratagene, La Jolla, CA, USA), with the following oligonucleotide primers (the underlined codon encodes the altered amino acid): 5′-ggtggtcttccgcatggtgctgacggctg-3′; 5′-cagccgtcagcaccatgcggaagaccacc-3′, as previously described (Orthmann-Murphy *et al*., 2007*a*). The resulting DNA [in pIRES2-EGFP and subcloned into pIRESpuro3 (Clontech, Mountain View, CA, USA)] and the mutation was confirmed by sequencing at the Sequencing Core of the University of Pennsylvania.

Neuro2A cells (N2A, from American Type Culture Collection, Manassas, VA, USA) and communication-incompetent HeLa cells (gift of Dr Klaus Willecke, University of Bonn, Bonn, Germany) were maintained and transfected to transiently or stably express mutant or WT Cx47 as previously described (Orthmann-Murphy *et al*., 2007*a*, *b*). Heterotypic mix experiments were performed on HeLa cells stably expressing WT Cx43, WT Cx47, I33M or P87S as described previously (Orthmann-Murphy *et al*., 2007*b*).

Cells were immunostained as previously described (Orthmann-Murphy *et al*., 2007*a*, *b*) using rabbit antisera raised against the C-terminus of human Cx47 [diluted 1:1500; (Orthmann-Murphy *et al*., 2007*a*)] or mouse monoclonal antibodies against mouse Cx43 (diluted 1:1000; Millipore Corporation, Billerica, MA, USA) or pan-cadherin (Novus Biologicals, Littleton, CO, USA; diluted 1:200) and FITC-, TRITC-, and Cy5-conjugated secondary antibodies. Images were acquired using a Leica fluorescence microscope and Openlab 3.1.7 or a FluoView FV1000 Olympus laser scanning confocal microscope (60×, oil immersion objective). Confocal images were merged and pseudocoloured using Image J 1.37v (National Institutes of Health, USA) then imported into Adobe Photoshop (San Jose, CA, USA) for post-processing. Transfected HeLa and N2A cells were collected and processed for immunoblotting as previously described (Orthmann-Murphy *et al*., 2007*a*).

Functional tests of the I33M mutant

Confluent HeLa cell monolayers were scrape loaded as previously described (Orthmann-Murphy *et al*., 2007*a*). We used dual whole-cell patch clamping to assess formation of both homotypic channels, on pairs of N2A cells transiently transfected with WT Cx43, WT Cx47 or I33M subcloned into pIRES2-EGFP, and heterotypic channels, on pairs of cells each expressing a pIRES2-EGFP construct or pIRES2-DsRed construct, as described previously (Orthmann-Murphy *et al*., 2007*b*). Recording solutions used were as follows (in mM): pipette solution, 145 $CsCl_2$, 5 EGTA, 0.5 $CaCl_2$ and 10.0 HEPES, pH 7.2; bath solution, 150 NaCl, 4 KCl, 1 $MgCl_2$, 2 $CaCl_2$, 5 dextrose, 2 pyruvate and 10 HEPES, pH 7.4. Heterotypic pairings between two cells are shown as 'connexin expressed in cell 2/connexin expressed in cell 1'; junctional conductance (G_j)—junctional voltage (V_j) relations were determined from isolated pairs by measuring instantaneous junctional current (I_j) responses in cell 2 following 12.5-s V_j pulses (from −100 to 100 mV in 20 mV increments) applied to cell 1 and applying Ohm's law. Baseline G_j was similarly determined by measuring instantaneous I_j responses to ±40 mV V_j pulses.

Statistical analyses

For heterotypic mix experiments, epifluorescence images were imported into Adobe Photoshop and analysed as previously described (Orthmann-Murphy *et al*., 2007*b*). At least 11 DsRed + cells from two cover slips were analysed for each heterotypic mixture; this was repeated in three independent experiments. For each DsRed + cell, we determined the mean and 95% CI of the number of overlapping cell surface puncta. The number of DsRed + cells with or without one or more overlapping puncta was compared using Fisher's exact test with Bonferroni's correction for multiple comparisons. All statistical tests were performed in GraphPad Prism (San Diego, CA, USA). For dual whole-cell patch clamp assays, values are presented as mean $G_j \pm$ SEM, and were compared using Fisher's exact test or Mann–Whitney test in GraphPad Prism.

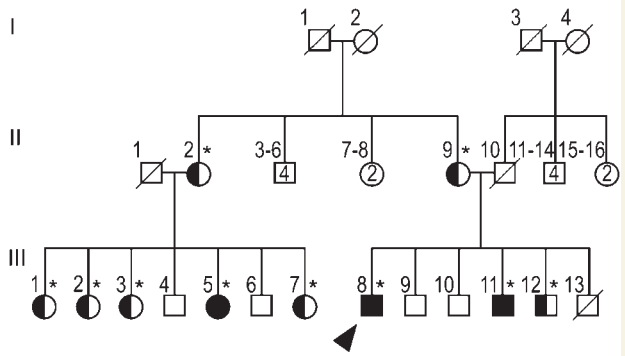

Fig. 1 Family pedigree. The family pedigree is shown, and the genotypes were determined for all individuals indicated by asterisks. The proband (III-8; arrowhead), III-11 and III-5 are homozygous for the I33M mutation; II-2, II-9, III-1, III-2, III-3, III-7, and III-12 are asymptomatic heterozygous carriers, and II-9, III-7, and III-12 have normal neurological exams. The other family members were not tested for the mutation and were reported to be neurologically normal. Subjects I-2, I-3 and II-1 had the same surname, suggesting possible consanguinity. Note that unaffected family members of the same gender are grouped together in generation II (e.g. subjects II-3, II-4, II-5 and II-6 are four unaffected males).

Results

Clinical findings

The family pedigree is shown in Fig. 1. There were three affected members—the proband (III-8, arrowhead), his brother (III-11) and their female cousin (III-5). At age 39, the proband presented with an 8-year history of slowly progressive walking difficulties, leg stiffness and slurred speech. He felt 'awkward' since his school years, had minimal writing difficulties, but was fit for military service at age 18. At age 21, he underwent surgery for concomitant strabismus. Currently, he is able to walk without assistance, and works as a priest. His legs and gait were spastic, and bilateral Babinski signs were found. The jaw jerk and deep tendon reflexes (DTRs) were brisk throughout, with non-sustained ankle clonus. Mild pes cavus was noted. He had no nystagmus, but pursuit eye movements were slightly saccadic. The following findings were mild: pseudobulbar dysarthria, loss of finger dexterity, dysmetria and intention tremor on finger-to-nose and heel-to-knee testing.

The proband's 36-year-old brother (III-11) had minimal motor difficulties since infancy and mild learning impairment at school. He reported mild intention tremor during late-childhood, and a few tonic-clonic seizures, mainly febrile, between childhood and his early teens. These problems had long been attributed to a dystocic delivery with cyanosis at birth. After age 20, he began to show a slow worsening of walking difficulties and slight dysarthria, followed by decreased dexterity with his hands. Presently, he walks with a cane, but he can still walk a few steps without aid. On neurological examination he had a shuffling, scissor-like gait, marked spasticity with mild weakness of the lower limbs, an increased jaw jerk and increased DTRs in all limbs, with sustained clonus at the ankles and bilateral Babinski signs. He had slight

Table 1 Summary of clinical and instrumental data for patients with the I33M *GJA12/GJC2* mutation

	Patient III-8	Patient III-11	Patient III-5
Sex/Age at examination (years)	M/39	M/36	F/53
Age at disease onset	2nd decade	1st decade	1st decade
Age of disease progression (years)	>30	>20	>10
Initial motor development	Normal	Normal	Walking at 2 yrs
Onset symptom	Difficulty in walking	Hand tremor	Difficulty in walking
Walking ability at exam	Without aid	With unilateral aid	Chairbound since age 30
Lower limb spasticity	++	+++	++++
Upper limb motor involvement	±	+	++
Dysarthria	+	++	++
Nystagmus	–	–	–
Cerebellar ataxia	±	+	++
Mental impairment/IQ score	±/94	±/83	+/77
Epilepsy	–	+	–
Sphincter dysfunction	–	–	++
Sensory loss	–	–	++
Sensorineural hearing loss	–	–	+
Other signs	Pes cavus, strabismus	Pes cavus, strabismus	Pes cavus, scoliosis
MRI	Hypomyelination	Hypomyelination	Hypomyelination and atrophy
^{1}H-MRSI	↓Cho/NAA, Cho/Cr ratios	↓Cho/NAA, Cho/Cr ratios	↓Cho/NAA, Cho/Cr ratios
EEG	Near-normal	Near-normal	Near-normal
EMG and nerve conduction studies	Normal	Normal	Normal
VEPs, BAEPs, MEPs and SEPs	Abnormal	Abnormal	Abnormal
Autonomic tests	Normal	ND	ND

–absent; ± = minimal; + = mild; ++ = moderate; +++ = marked; ++++ = severe; ND = not done. BAEPs = brainstem auditory evoked potentials; EMG = electromyography; MEPs = motor evoked potentials; SEPs = somatosensory evoked potentials; VEPs = visual evoked potentials.

dysarthria, mild loss of finger dexterity, dysmetria, intention tremor on finger-to-nose testing and moderate hypodiadochokinesia. He had pes cavus with hammer toes, lumbar hyperlordosis and concomitant strabismus but no nystagmus.

The proband's 53-year-old cousin (III-5) had always been considered somewhat dull, but completed primary school without help. She walked at 20 months, and developed progressive spastic paraplegia and dysarthric speech beginning in her teens, becoming wheelchair bound at age 30. She later developed urinary incontinence followed by retention, and required a permanent catheter at age 46. More recently, she has developed episodic painful spasms in lower limbs, and marked constipation with rare fecal incontinence. On exam, she was unable to stand or walk without bilateral support. Her arms were mildly spastic, atrophied and weak; her legs were markedly spastic, wasted and completely paralysed. Her jaw jerk and all DTRs were exaggerated, with sustained right ankle clonus and bilateral Babinski signs. She had slightly saccadic pursuits without nystagmus, and moderate dysarthria with nasal, scanning and spastic qualities. She had moderate dysmetria and intention tremor on finger-to-nose testing, with marked hand hypodiadochokinesia. Light touch and pain sensations were reduced in the left upper limb and both legs. Position and vibration sense were severely impaired in the legs. She also had severe dorsal scoliosis, bilateral pes cavus and ankle contractures (Table 1).

Clinical investigations

The following blood tests were normal for all affected patients: creatine kinase, uric acid, ammonia, lactate, pyruvate, alanine and other amino acids, very-long-chain fatty acids and phytanic acid. Urinary levels of organic acids, amino acids and sulfatides were also normal. Lysosomal enzyme assessment in blood leukocytes ruled out metachromatic leukodystrophy, Krabbe disease and GM1 and GM2 gangliosidoses. Neuro-ophthalmologic examination revealed only left eye amblyopia in patients III-8 and III-11, attributed to congenital strabismus. Audiometry revealed mild sensorineural hearing loss in Patient III-5 and left ear conduction hypoacusia due to previous trauma in Patient III-8.

Electromyography and motor and sensory nerve conduction studies were normal in all three patients. Motor evoked potential (MEP) studies showed prolongation of central motor conduction time (CMCT) in upper limbs, and no response in lower limbs in Patients III-8 and III-11; in Patient III-5, MEPs could be recorded only from the left upper limb, with central motor conduction time prolongation, whereas no response was obtained from the other limbs. Their electroretinogram was normal, whereas visual evoked potentials showed delayed P100 wave latencies. Brainstem auditory evoked potentials disclosed absence or severe distortion and delay of waves III and V; wave I was normal in Patients III-11 and III-5, but almost unrecognizable in Patient III-8, particularly on the left side. Upper and lower limb somatosensory evoked potential studies demonstrated delayed latencies of central components in all patients; no response could be evoked in lower limbs in Patient III-5. In all patients, EEG showed a posterior background activity of about 8 Hz with a slightly irregular morphology. The cardiovascular reflexes were normal in Patient III-8. Neuropsychological assessment revealed IQ scores of 94 in Patient III-8, 83 in Patient III-11 and 77 in Patient III-5 (normal value > 70).

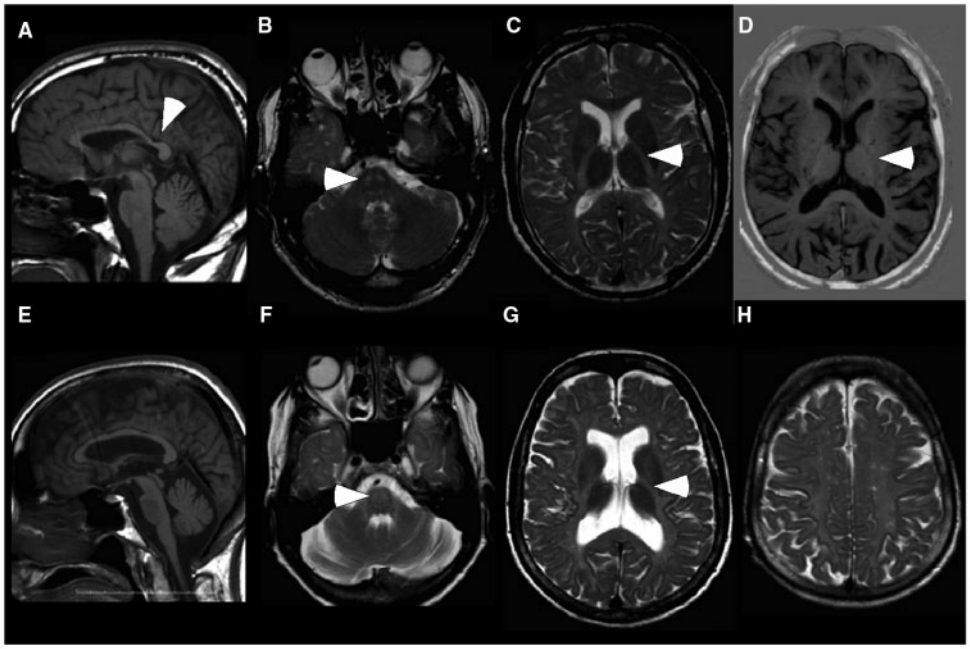

Fig. 2 Imaging studies show white matter abnormalities. These are MRI images from patients III-8 **(A–D)** and III-5 **(E–H)**. Sagittal T_1-weighted (T_1W) images [spin-echo (SE): repetition time (TR)/echo time (TE) 556/13 ms; 6-mm thickness] shows thinning of the corpus callosum, posteriorly (**A**, arrowhead) or diffusely **(E)**. Axial T_2W images (SE: TR/TE = 3200/90 ms; 5-mm thickness) show symmetric hyperintensity in the region of the corticospinal/corticobulbar tracts at the level of the pons **B** and **F**, arrowhead) and the posterior limb of internal capsule (**C** and **G**, arrowhead). In addition, there is diffuse hyperintensity in the subcortical, lobar and periventricular white matter **(C, G** and **H)**, and enlarged ventricles, especially in Patient III-5 **(G)**. Axial T_1W image [inversion recovery turbo spin-echo (IRTSE): TR/TE = 5600/70 ms; flip angle 150°; 4-mm thickness] shows diffuse hypointensity in the white matter, including the posterior limb of the internal capsule (**D**, arrowhead).

Brain MR imaging and spectroscopic findings were homogeneous in the three patients and highly suggestive of a hypomyelinating leukoencephalopathy. White matter regions showed diffuse high signal intensity on T_2-weighted and low signal on T_1-weighted images (Fig. 2, Supplementary Fig. 1). T_2-weighted signal hyperintensity was evident at level of the pons, in the region of corticospinal and spinothalamic tracts (Fig. 2B and F). The corpus callosum was thin in all patients. The cervical spine of Patient III-8 appeared normal (data not shown). Ventricular and posterior fossa dilation, likely secondary to white matter volume loss, was mild in Patients III-8 and III-11, but advanced in Patient III-5. Choline (Cho), *N*-acetyl-aspartate (NAA) and creatine (Cr) were measured in the white matter of the centrum semiovale by ^{1}H MR spectroscopic imaging. The NAA/Cr ratios were within normal values, consistent with what has been reported for PMD and PMLD (Lee *et al*., 2004; Bizzi *et al*., 2008). Average Cho/NAA and Cho/Cr ratios, however, were reduced—0.49 and 0.84 in Patient III-8; 0.47 and 0.80 in Patient III-11; 0.44 and 0.75 in Patient III-5—compared with 0.60 and 1.0, respectively, in normal adults.

Affected patients have an I33M mutation in *GJA12/GJC2*

The above data indicated that the three patients from this family had a recessively inherited hypomyelinating leukoencephalopathy with an unusual clinical phenotype of a late onset complicated HSP. Although the parents of our patients were reported to be unrelated, they all originated from a small village in northern Italy, and Subjects I-2, I-3 and II-1 (Fig. 1) had the same family name. Hence, we sequenced amplified genomic DNA of the *GJA12/GJC2* gene, and found a novel missense mutation (99C > G), predicted to cause an Ile > Met amino acid substitution (I33M) in Cx47. This mutation was homozygous in the three affected individuals, heterozygous in obligate healthy carriers and some clinically normal relatives (asterisks in Fig. 1 denote DNA analysis), and absent in 210 control alleles. Heterozygous relatives (Fig. 1) were asymptomatic and had a normal neurological exam (II-9, III-7 and III-12); one of these relatives (III-7) had a normal brain MRI and ^{1}H MRSI.

As shown in Fig. 3, I33 is located in the first transmembrane domain, which is a highly conserved region of connexins (Yeager and Nicholson, 1996). This amino acid residue is identical in Cx47 orthologues of other vertebrates (cow, mouse, frog and zebrafish; Supplementary Fig. 2), but Val (Cx30, Cx30.3, Cx31, Cx31.1), Leu (Cx30.2) or even Met (Cx40, Cx59, Cx62) are found at the corresponding position in other connexins (Supplementary Fig. 2). Although mutations in the genes encoding Cx26, Cx30, Cx30.3, Cx31, Cx32, Cx40, Cx43, Cx46 and Cx50 have been described, mutations in the residues corresponding to I33 have not been identified previously.

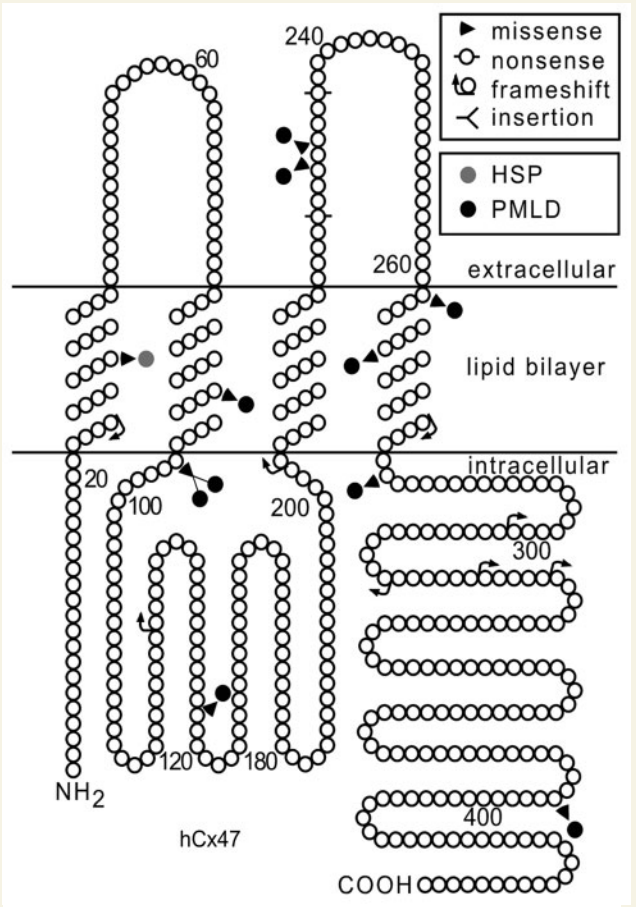

Fig. 3 *GJA12/GJC2* mutations associated with CNS diseases. This is a schematic drawing of human Cx47, illustrating the position and nature of mutations associated with CNS diseases. I33M (grey circle) is located in the first transmembrane domain. All of the other mutations depicted cause PMLD (black circles), either as homozygous mutations or as compound heterozygote mutations (missense mutations: P87S, G146S, G233R, G233S, T262A, Y269D, M283T and T395I; frameshift mutations: L25fs, P128fs, E204fs, L278fs, P302fs, C315fs, A322fs and P327fs; non-sense mutations: Y229stop and R237stop; complex mutations: A95G____V96insertT) (Uhlenberg *et al*., 2004; Bugiani *et al*., 2006; Salviati *et al*., 2007; Wolf *et al*., 2007; Henneke *et al*., 2008). The positions of the transmembrane domains are based on the work of Yeager and Nicholson (Yeager and Nicholson, 1996).

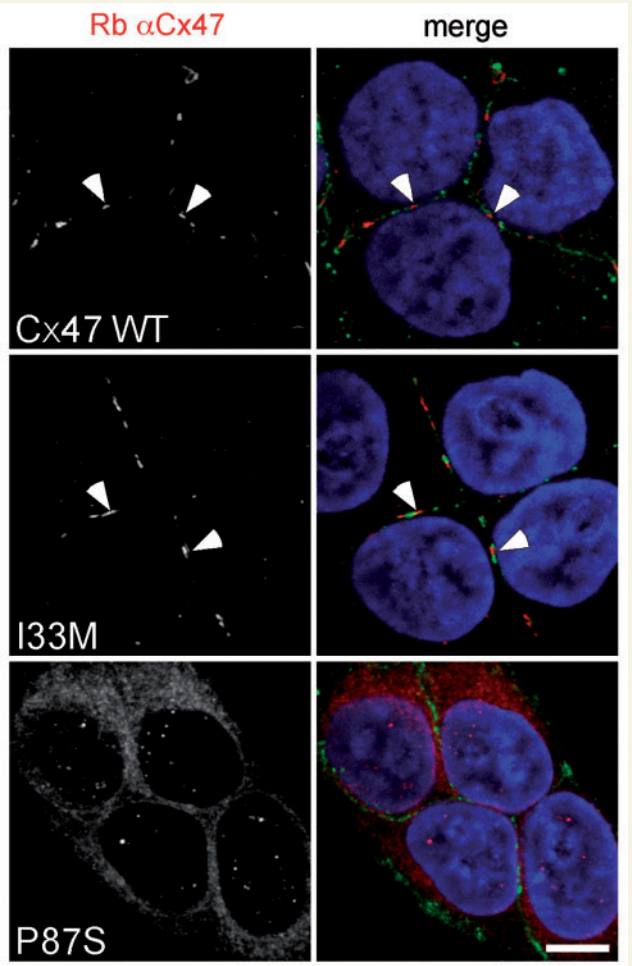

Fig. 4 The I33M mutant forms gap junction plaques. These are confocal images of bulk-selected HeLa cells that express WT Cx47 or the indicated mutants, immunostained with a rabbit antiserum against human Cx47 (red) and a mouse monoclonal antibody against pan-cadherin (green), and counterstained with DAPI. The pan-cadherin staining at cell borders interdigitates with the cell surface staining of Cx47 in cells that express WT Cx47 (arrowheads) or I33M (arrowheads), but surrounds the staining of cells expressing the mutant P87S, which is localized in the endoplasmic reticulum. Scale bar: 10 μm.

I33M forms gap junction plaques in HeLa cells

To investigate the underlying molecular defects of the I33M mutant, we expressed it in communication-incompetent HeLa and N2A cells. For comparison, we also expressed WT Cx47 and P87S, a missense mutant that causes PMLD (Uhlenberg *et al*., 2004), and results in loss-of-function (Orthmann-Murphy *et al*., 2007*a*, *b*). We confirmed expression by immunoblotting lysates from bulk-selected and transiently transfected cells (Supplementary Fig. 3). As expected (Orthmann-Murphy *et al*., 2007*a*, *b*), P87S was localized the endoplasmic reticulum (ER) in both transiently (Supplementary Figs. 4 and 5) and permanently transfected (Fig. 4) cells, whereas I33M (and WT Cx47) formed gap junction plaques at apposed cell borders. We confirmed the cell surface localization of WT Cx47 and I33M by double labelling with a monoclonal antibody that recognizes cadherins. Neither parental HeLa cells, nor bulk-selected HeLa cells that had been transfected to express vector alone, expressed Cx47 (data not shown). We obtained similar results in four separate transient transfection experiments and two different bulk-selected cell lines expressing I33M.

I33M does not form functional homotypic channels

Because patients expressing I33M have a milder phenotype than do patients with PMLD, and I33M can form gap junction plaques,

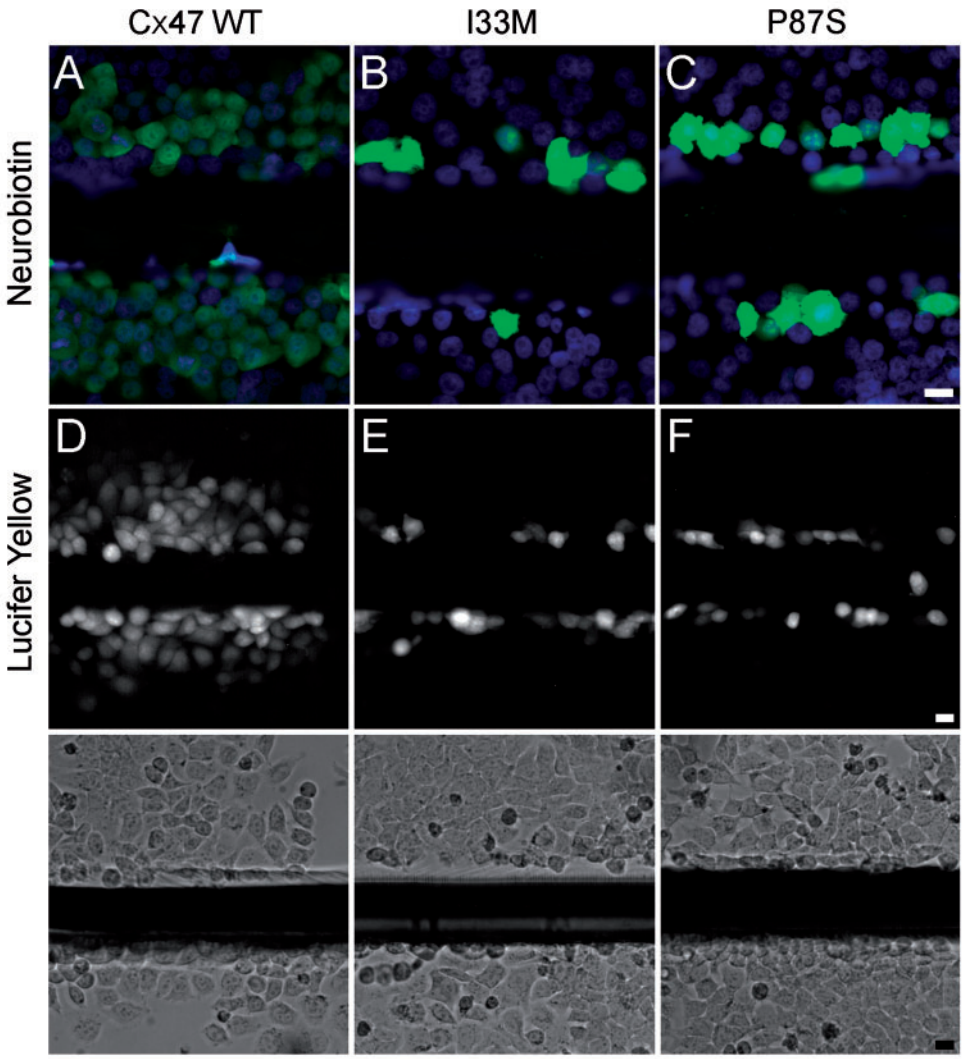

Fig. 5 I33M is impermeable to low molecular weight tracers. These are representative images of bulk-selected HeLa cells that stably express WT Cx47 or the indicated mutants, scrape-loaded with neurobiotin **(A—C)** or Lucifer Yellow (**D—F)**. Cells scrape-loaded with neurobiotin were fixed with 4% paraformaldehyde, then visualized using FITC-conjugated extravidin (green) and DAPI counterstain (blue). Cells scrape-loaded with Lucifer Yellow were imaged by epifluorescence (top row) and phase contrast (bottom row) 5 min after scrape loading. Only HeLa cells expressing WT Cx47 showed transfer of neurobiotin (**A)** or Lucifer Yellow (**D)** to neighbouring cells. The images for each type of scrape loading experiment were acquired on the same day at the same exposure. (**A—C)** scale bar: 20 μm; (**D—F)** scale bar: 20 μm.

we hypothesized that I33M might form gap junction channels with altered functional properties. To determine whether I33M could transfer small molecules, we scrape loaded cells (el-Fouly *et al*., 1987; Trosko *et al*., 2000), using gap junction tracers of different sizes, shapes and charge. A confluent monolayer of cells was injured with a scalpel blade in media that contained 2% neurobiotin (NB; MW 287, +1) or 0.1% Lucifer Yellow (LY; MW 443, −2). As in parental cells or cells expressing vector alone (data not shown), no transfer was seen past the scrape line in bulk-selected cells expressing I33M or P87S (Fig. 5B–C and E–F), whereas NB and LY transferred to cells beyond the scrape line for cells expressing WT Cx47 (Fig. 5A and D). We also confirmed that the cells along the scrape line expressed the appropriate connexin (Supplementary Fig. 6). This experiment was repeated at least twice in two different bulk-selected cells lines expressing I33M with similar results.

We used a more sensitive assay to determine whether Cx47 mutants can form functional homotypic gap junctions—dual whole-cell patch clamping on transiently transfected N2A cells. In this experiment, each cell was transiently transfected to express a single connexin as well as EGFP. For negative control pairs, cells expressing a single connexin were paired with cells expressing EGFP alone (Cx/EGFP). Voltage ramps or steps were applied to one cell of an EGFP-expressing pair, and current responses were measured in the second cell; the junctional voltage (V_j) corresponds to the difference in voltage between the two cells. As shown in Table 2, I33M/I33M homotypic pairings failed to form functional channels (0/6 pairs), whereas cell pairs expressing

Table 2 Summary of dual whole-cell patch clamp recordings

	n	Mean G_j (nS)	SD	SEM
I33M/I33M	6	0	0	0
I33M/Cx47	15	0	0	0
Cx47/Cx47	5	19.31	23.58	10.55
I33M/Cx43	13	0.05	0.13	0.04
Cx47/Cx43	3	23.50	29.12	16.81
I33M/DsRed	6	0	0	0
Cx47/EGFP	4	0.03	0.05	0.03
Cx43/EGFP	3	0.50	0.87	0.50

N2A cells transiently expressing WT Cx43, WT Cx47 or I33M were paired as noted; using dual whole-cell patch clamping, junctional conductance (G_j) was measured when junctional voltage (V_j) was zero. No coupling was detected between pairs of cells either each expressing I33M (I33M/I33M) or separately expressing I33M or WT Cx47 (I33M/Cx47). Extremely low levels of coupling were detected between pairs of cells separately expressing I33M or WT Cx43 (I33M/Cx43). SEM=standard error of the mean; DsRed=pIRES2-DsRed monomer; EGFP=pIRES2-EGFP.

WT Cx47 were coupled. The difference between I33M/I33M and WT Cx47/Cx47 pairings was statistically significant (I33M/I33M versus Cx47/Cx47, $P=0.0022$, Fisher's exact test). Thus, I33M does not appear to form functional homotypic gap junctions by two different assays.

I33M forms functional heterotypic channels with Cx43 in a cell model system

To determine whether I33M can form heterotypic channels with Cx43, we applied morphological and functional assays we used previously to show that Cx47 mutants associated with PMLD do not form functional heterotypic gap junctions with WT Cx43 (Orthmann-Murphy *et al*., 2007*b*). In the morphological assay, cell lines in which at least 90% of cells stably expressed Cx47 (I33M, P87S or WT Cx47) or Cx43 were transiently transfected to express DsRed (DsRed + cells). The DsRed + cells (expressing Cx47 or Cx43) were mixed with DsRed- cells (expressing Cx43 or Cx47, respectively) at a ratio of 1:20, and, 24 h after plating, immunostained for Cx47 and Cx43. For each combination, we determined whether the connexin puncta at the periphery of the DsRed + cell overlapped with connexin puncta expressed by the surrounding DsRed- cells. As shown in Fig. 6, P87S was localized to the ER, and did not appear to form overlapping puncta with Cx43 (Orthmann-Murphy *et al*., 2007*b*). In contrast, cells expressing I33M or WT Cx47 formed overlapping puncta with Cx43, suggesting that I33M/Cx43 may form functional channels. We quantified these results by counting the number of puncta at the cell membrane of each central DsRed + cell, and determining whether these puncta overlapped with the connexin signal in the surrounding DsRed- cells (Fig. 6D). In this analysis, the mixtures are designated as 'CxA*/CxB,' where the asterisk denotes the connexin expressed by the DsRed + cell. Mixtures containing I33M/Cx43 (I33M*/Cx43 and Cx43*/I33M) produced a significantly larger proportion of DsRed + cells with at least one overlapping punctum than did P87S/Cx43 mixtures (I33M*/Cx43 versus P87S*/Cx43 or Cx43*/P87S, Cx43*/I33M versus P87S*/Cx43, $P<0.0001$; Cx43*/I33M versus Cx43*/P87S, $P=0.0013$, Fisher's test), but were not significantly different than mixtures containing Cx47/Cx43 (Cx47*/Cx43 and Cx43*/Cx47).

In the electrophysiogical assay, we used dual whole-cell patch clamping on pairs of N2A cells. In these experiments, each cell was transiently transfected to express a single connexin as well as EGFP or monomeric DsRed, so that each member of a cell pair could be unambiguously identified. To confirm that the cells expressing EGFP or DsRed also expressed the expected connexin, we immunostained transiently transfected cells (Supplementary Fig. 5). In this way, we previously showed that three loss-of-function Cx47 mutants that cause PMLD (P87S, Y269D and M283T) do not form functional heterotypic channels with Cx43 (Orthmann-Murphy *et al*., 2007*b*). In contrast, we detected I_j activation for six of 13 (46%) I33M/Cx43 pairs tested, somewhat less than we previously found for all of the WT Cx47/Cx43 heterotypic pairs we have tested (40 of 55; 73%). As shown in Table 2, the mean G_j measured at $V_j = 0$ for I33M/Cx43 channels is significantly smaller than that of WT Cx47/Cx43 channels (I33M/Cx43 versus WT Cx47/Cx43, $P<0.05$, Mann–Whitney test). Negative control pairs, in which cells expressing a single connexin were paired with cells expressing EGFP or DsRed alone, showed low levels of coupling probably due to formation of heterotypic channels with an endogenous connexin expressed by parental N2A cells (Table 2; Orthmann-Murphy *et al*., 2007*b*).

To better define the functional differences between I33M/Cx43 and Cx47/Cx43 channels, we examined macroscopic current responses and G_j–V_j relations. By convention, pairing designation is 'connexin expressed by cell 2/connexin expressed by cell 1'. Both cells in the pair were voltage clamped to 0 mV; cell 1 was stepped between −100 and 100 mV in 20 mV increments, and current was recorded from cell 2. For I33M/Cx43 heterotypic pairings, negative pulses ($\leqslant -40$ mV) applied to the cell expressing Cx43 activate junctional currents (I_j) (Fig. 7A). Assuming that G_j is a linear function of V_j between −20 mV and +20 mV, the normalized G_j versus junctional voltage (V_j) relation reveals that I33M/Cx43 channels are about fifty times more likely to be open after a 12.5-s pulse to $V_j = -100$ mV than at $V_j = 0$ mV (solid line, Fig. 7B). This is strikingly different than WT Cx47/Cx43 channels (dashed line), which are more likely to be open at $V_j = 0$ mV than at either −100 mV or + 100 mV (Fig. 7B; Orthmann-Murphy *et al*., 2007b). The left shift of the G_j–V_j relation for I33M/Cx43 channels is likely explained by an extremely low open probability of the I33M hemichannel when $V_j < -40$ mV are applied to the cell expressing Cx43; this can account for the significantly reduced G_j values detected at $V_j = 0$ mV for both I33M/Cx43 and I33M/I33M channels (Table 2). Although the WT Cx43 hemichannel has negative V_j gating polarity (Bukauskas *et al*., 2001) and should be closed under the conditions that open I33M hemichannels, Cx43 rarely closes fully (Bukauskas *et al*., 2000). It is possible, then, that I33M is forming a channel with a substate of Cx43. Properties of I33M/WT Cx47 channels (in 5/15 pairs) are similar to those described for I33M/Cx43 (data not shown).

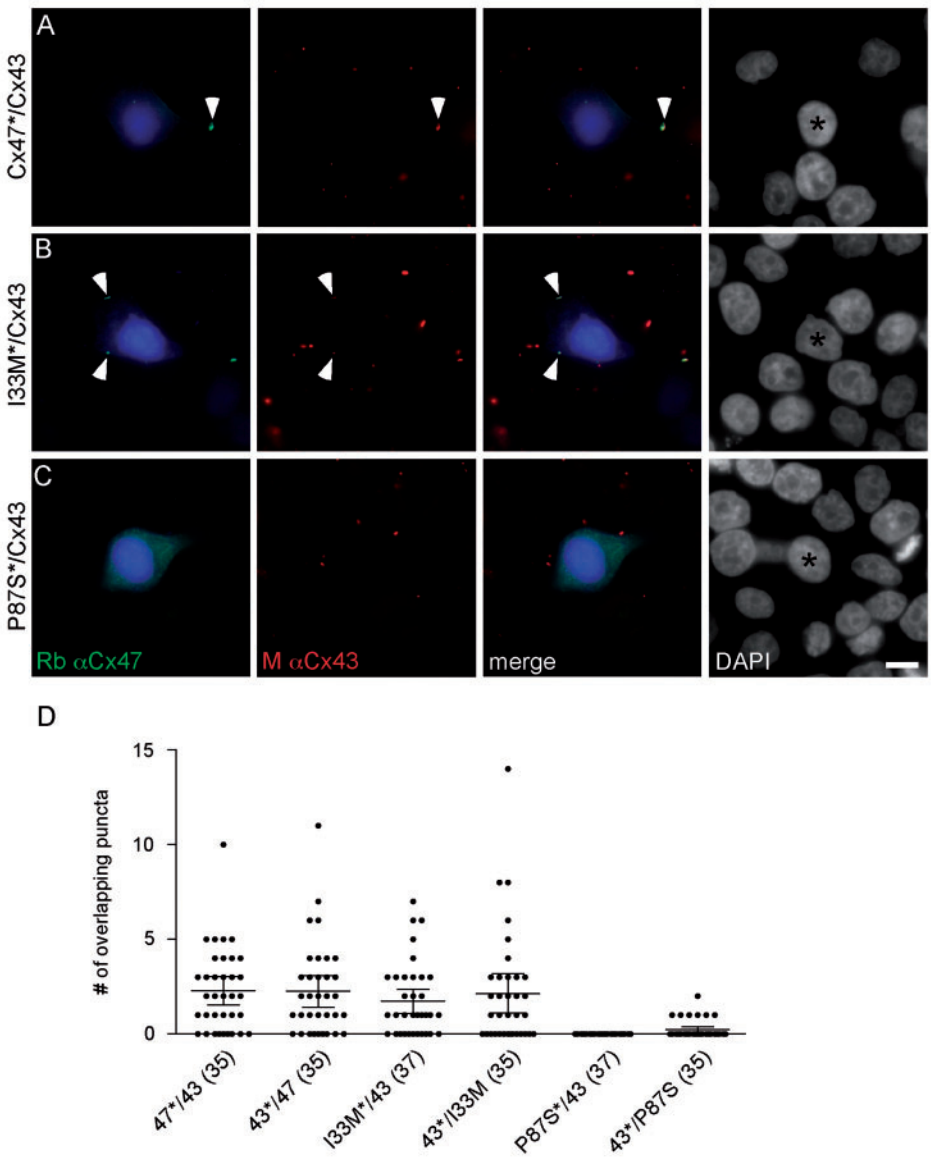

Fig. 6 I33M/Cx43 pairings form gap junction plaques. **(A–C)** HeLa cells stably expressing Cx47 WT or one of the mutants (I33M or P87S) or Cx43 were transiently transfected to express DsRed (DsRed+) and mixed with cells expressing one of the connexins, but not transfected with DsRed (DsRed−), in a ratio of 1:20, respectively. After 24 h, cells were immunostained as indicated and counterstained for DAPI. One of the two possible pairings for each combination is illustrated. The DsRed+cell is pseudocoloured blue in the first and third columns, and indicated by an asterisk in the fourth column. Note that I33M/Cx43 (**B**) pairings have overlapping puncta at the border of the DsRed signal (arrowhead) similar to Cx47/Cx43 pairings **(A)**, whereas P87S/Cx43 pairings **(C)** do not. **(D)** Quantitative summary of three independent experiments such as illustrated in **(A–C)**. The asterisk denotes the DsRed+cell. Each dot represents the number of overlapping puncta determined for 1 DsRed+cell. In each column, the horizontal bar denotes the mean, the vertical bar represents the 95% confidence interval, and the total number of DsRed+cells is shown in parentheses. Both pairings of I33M/Cx43 (I33M*/43 and 43*/I33M) have overlapping puncta similar to pairings of Cx47/Cx43 (47*/43 and 43*/47). Results for Cx47/Cx43 and P87S/Cx43 pairings are similar to those previously reported (Orthmann-Murphy et al., 2007*b*).

Discussion

The I33M Cx47 mutant causes hereditary spastic paraplegia

The three patients with a homozygous 99C>G mutation in *GJA12/GJC2* all developed HSP, characterized by a progressive gait disorder during the first to fourth decades of life. The proband exhibited an almost pure spastic paraplegia with mild ataxia and dysarthria, and walked unaided at age 39. His brother had moderately complicated spastic paraplegia, with mild ataxia and dysarthria, a few seizures and walked with unilateral support at age 36. Their cousin had a more severe and complex phenotype, with earlier onset and became wheelchair dependent at age 30. The late onset, preserved ability to walk unaided until adulthood, and

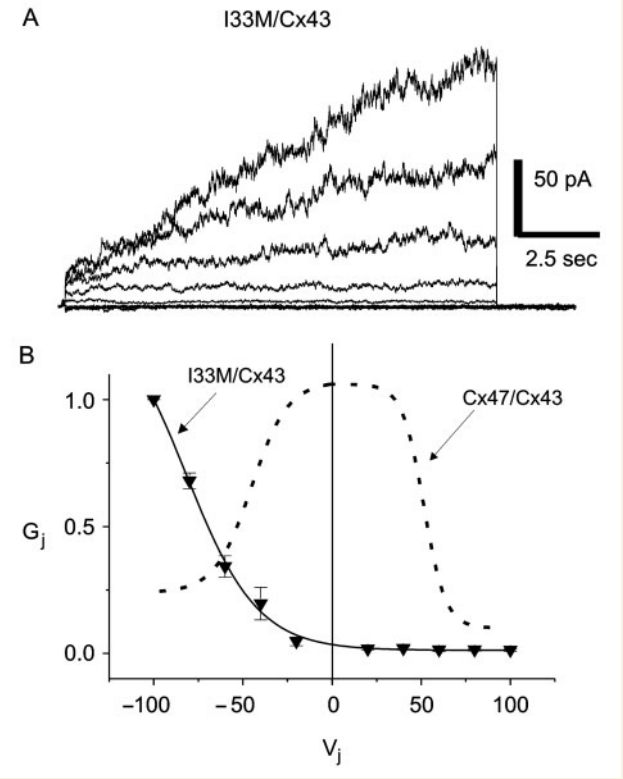

Fig. 7 Functional properties of I33M/Cx43 channels. N2A cells were transiently transfected with a pIRES2-EGFP or a pIRES2-DsRed bicistronic expression vector that also contained WT Cx43 or I33M. After 24 h, red and green cell pairs were generated by mixing the transfected cells at a 1 to 1 ratio, and assessed by dual whole-cell patch clamping 24–48 h later. **(A)** These are representative current traces recorded from an I33M/Cx43 pairing; both cells were voltage clamped to 0 mV and the cell expressing WT Cx43 was stepped in 20 mV increments from $V_j = -100$ to $V_j = 100$ mV, and junctional current (I_j) was recorded from the cell expressing I33M. Note that the polarity of I_j is opposite that of V_j. Current responses were only activated when a pulse less than or equal to −40 mV was applied to the Cx43-expressing cell. Traces were filtered at 200 Hz. **(B)** Average normalized G_j–V_j relations for heterotypic I33M/Cx43 channels (solid line) and WT Cx47/Cx43 channels (dashed line). For I33M/Cx43 channels, the average $G_j \pm$ SEM at each V_j (filled triangles) was calculated from current traces such as those shown in **(A)** and normalized to the value at –100 mV. The WT Cx47/Cx43 channel trace is from Orthmann-Murphy et al., 2007*b*. Note that I33M/Cx43 channels are only open when V_j is less than −40 mV, and are closed when WT Cx47/Cx43 channels are open ($V_j = 0$ mV). Each point in the G_j–V_j plot is the average of data from three independent experiments.

absence of nystagmus clearly distinguish these patients from the more severe PMLD phenotype caused by other recessive mutations in *GJA12/GJC2* (Fig. 3). These PMLD patients typically present by 12 months of age with nystagmus and impaired psychomotor development, and rarely walk unaided in childhood (Uhlenberg *et al*., 2004; Bugiani *et al*., 2006; Salviati *et al*., 2007; Wolf *et al*., 2007; Henneke *et al*., 2008).

The diffuse white matter MR signal abnormalities and mildly altered ^{1}H MRSI metabolic profiles in the three patients homozygous for the I33M mutation suggested a hypomyelinating leukoencephalopathy, which is consistent with oligodendrocyte expression of Cx47. In our adults patients, the T_2-signal abnormalities were more subtle than those shown for previously reported PMLD patients (caused by *GJA12/GJC2* mutations), who ranged in age from 5 months to 12 years (Uhlenberg *et al*., 2004; Bugiani *et al*., 2006; Salviati *et al*., 2007; Wolf *et al*., 2007). Notably, T2-signal hyperintensity for patients with the I33M mutation was discrete and prominent in the corticospinal and spinothalamic tracts (especially at the level of the pons). A similar involvement of these tracts is evident in the MR images of spastic PMLD patients reported by Wolf and colleagues (2007), whereas the corticospinal tracts appeared to be relatively spared in PMLD patients with other *GJA12/GJC2* mutations (Bugiani *et al*., 2006). In our patients, the involvement of the long white matter tracts may correlate with the severity of spastic paraplegia. The mild decrease in metabolite ratios (Cho/NAA and Cho/Cr) measured in our patients, and previously reported for one of two PMLD patients with *GJA12/GJC2* mutations (Bugiani *et al*., 2006), are in agreement with a recent study suggesting that hypomyelinating disorders (including PMLD due to *GJA12/GJC2* mutations) are associated with normal or near-normal metabolite ratios, compared to a large increase in choline or decrease in NAA typically seen in actively demyelinating leukoencephalopathies (Bizzi *et al*., 2008). Finally, like PMLD patients with *GJA12/GJC2* mutations, our patients exhibited central conduction slowing without electrophysiological evidence for peripheral neuropathy.

Hereditary spastic paraplegias are a heterogeneous group of genetic disorders characterized by progressive lower limb spasticity (pure HSP) that may be associated with other neurological abnormalities (complicated HSP; Fink, 2006). We propose that autosomal recessive mutations in *GJA12/GJC2* that cause HSP should be termed SPG44 (http://www.genenames.org). The patients described here have a slowly progressive disease consisting of a spastic paraplegia; the inclusion of minimal to moderate ataxia and dysarthria, and seizures suggest that they have a complicated HSP. Although some of the clinical findings indicate that the pathophysiology is not limited to the longest CNS axons, other forms of 'complicated' HSP have comparable, or even more severe, findings (http://www.ncbi.nlm.nih.gov/sites/entrez?db=OMIM). Similarly, MRI abnormalities in the white matter, comparable to the ones we report, have been found in one patient with SPG2 (Lee *et al*., 2004). Thus, *GJA12/GJC2* is only the second example (*PLP1* is the other) of mutations that cause HSP in a gene that is primarily expressed by oligodendrocytes; the other HSP-causing loci are thought to primarily affect neurons/axons (Fink, 2006). Screening for *GJA12/GJC2* mutations, therefore, should be considered for patients and/or families that present with a complicated HSP phenotype and hypomyelinating leukoencephalopathic findings on MRI.

Like *PLP1*, mutations in *GJA12/GJC2* appear to cause a spectrum of CNS white matter disease, including HSP and PMD/PMLD. Based on the similar phenotypes caused by *PLP1* and *GJA12/GJC2* mutations, one suspects that other causes of the PMLD (and HSP with primarily white matter pathology) will turn

out to be caused by mutations in genes that primarily affect oligodendrocytes. One example of this may be mutations of *HSPD1* (the gene encoding the mitochondrial chaperonin, Hsp60), which cause either uncomplicated autosomal dominant SPG13 (Hansen *et al*., 2002) or an autosomal recessive lethal disease similar to connatal PMD (Magen *et al*., 2008).

The molecular pathogenesis of HSP and PMLD due to mutations in *GJA12/GJC2*

Because the patients with homozygous I33M mutations have a milder phenotype than do patients with PMLD, we predicted that I33M would have a partial loss-of-function, as compared to complete loss-of-function we found for Cx47 mutants that cause PMLD (Orthmann-Murphy *et al*., 2007*a*, *b*). Furthermore, because oligodendrocytes form gap junctions with adjacent astrocytes, we predicted that I33M would still form functional, but likely altered, channels with Cx43. The finding that I33M formed gap junction plaques with itself and with Cx43 is consistent with this hypothesis, and demonstrates that I33M oligomerizes into hemichannels that traffic to the cell surface (Kumar and Gilula, 1996), compared with the ER-retained Cx47 mutants which cause PMLD. The failure of I33M to transfer small molecules such as Lucifer Yellow or neurobiotin (in scrape loading assays), or to form detectable homotypic channels (by dual whole-cell patch clamping), argues against this hypothesis. Both the failure to detect I33M/I33M dye coupling or currents and the alterations in the I33M/Cx43 G_j–V_j relation are likely due to a shift of the open probability of the I33M hemichannel as a function of voltage, such that its open probability increases only when a large voltage difference ($V_j \leqslant -40$ mV) is applied with the respect to the cell expressing Cx43. Some disease-associated Cx32 mutants show similar alterations in voltage dependence and are also thought to lead to loss-of-function (Oh *et al*., 1997; Abrams *et al*., 2001). Because large voltage gradients that open I33M/Cx43 channels probably do not occur across O/A junctions, the I33M mutant should cause loss-of-function of these channels. Large O/A gradients would be particularly improbable if these cells are well coupled by Cx30/Cx32 channels (Orthmann-Murphy *et al*., 2007*b*, 2008). Consequently, similar to patients with *GJA12/GJC2* mutations that cause PMLD, it is unlikely that Cx47/Cx43 gap junctions contribute to O/A coupling in patients with homozygous I33M mutations.

If the I33M mutation completely disrupts gap junction coupling via Cx47/Cx43 channels like the Cx47 mutants that cause PMLD, then another mechanism must account for the milder phenotype in our three patients. One possibility is that Cx47 has functions in oligodendrocytes beyond forming functional O/A channels. Because Cx47 has a PDZ binding domain [and at least one binding partner, ZO-1; (Li *et al*., 2004)], it is possible that I33M, in particular, retains some important function (such as binding ZO-1) that requires proper localization at the cell surface. Along these lines, it is possible that like some other connexins (Prochnow and Dermietzel, 2008), Cx47 is required for cell adhesion, as shown for Cx26 and Cx43 in neuronal migration in developing cortex (Elias *et al*., 2007), and Cx32 and Cx43 in an *in vitro* aggregation assay (Cotrina *et al*., 2008). Another possibility is that the recessive Cx47 mutants that cause PMLD (P87S, Y269D, M283T) actually have dominant effects (that the I33M mutant does not have) that contribute to the more severe phenotype of PMLD. Because the P87S, Y269D and M283T mutants are mostly found in the ER, it seems unlikely that they would form an abnormal hemichannel on the cell membrane (Richardson *et al*., 2004; Dobrowolski *et al*., 2007). Alternatively, because they accumulate in the ER, these mutants could induce an unfolded protein response with deleterious effects, but we found no evidence for this possibility in a cell model system (Orthmann-Murphy *et al*., 2007*a*).

Finally, it is possible that Cx47 mutants associated with more severe phenotypes result in more axonal degeneration, independent of their effects on myelin. In the peripheral nervous system, mutations in genes expressed by Schwann cells (such as *GJB1, PMP22* and *MPZ*) cause demyelinating neuropathy; although the demyelination is Schwann cell autonomous, clinical disability correlates with the degree of axonal damage (Nave *et al*., 2007; Scherer and Wrabetz, 2008). The enlarged ventricles in Patient III-5 (who was the most severely affected) are likely a result of axonal loss; such secondary axonal degeneration probably contributes to progressive neurological deterioration in PMD (Inoue, 2005; Garbern, 2007), and multiple sclerosis (Bjartmar *et al*., 1999). In spite of its importance, it is unclear how axons are damaged in any of these demyelinating disorders; in the case of Cx47 mutants, it is possible that disrupted O/A coupling impedes K^+ buffering mediated by glial gap junctions (Menichella *et al*., 2006).

Supplementary material

Supplementary material is available at *Brain* online.

Funding

National Institutes of Health (NS050345 and NS050705 to C.K.A.) (NS55284 to S.S.S.); the National Multiple Sclerosis Society (to S.S.S.); Mariani Foundation (to G.U. and M.Z.).

References

Abrams CK, Freidin MM, Verselis VK, Bennett MVL, Bargiello TA. Functional alterations in gap junction channels formed by mutant forms of connexin 32: evidence for loss of function as a pathogenic mechanism in the X-linked form of Charcot-Marie-Tooth disease. Brain Res 2001; 900: 9–25.

Altevogt BM, Kleopa KA, Postma FR, Scherer SS, Paul DL. Cx29 is uniquely distributed within myelinating glial cells of the central and peripheral nervous systems. J Neurosci 2002; 22: 6458–70.

Altevogt BM, Paul DL. Four classes of intercellular channels between glial cells in the CNS. J Neurosci 2004; 24: 4313–23.

Bizzi A, Castelli G, Bugiani M, Barker PB, Herskovits EH, Danesi U, et al. Classification of childhood white matter disorders using proton MR spectroscopic imaging. Am J Neuroradiol 2008; 29: 1270–5.

Bjartmar C, Yin XH, Trapp BD. Axonal pathology in myelin disorders. J Neurocytol 1999; 28: 383–95.

Bruzzone R, White TW, Paul DL. Connections with connexins: the molecular basis of direct intercellular signaling. Eur J Biochem 1996; 238: 1–27.

Bugiani M, Al Shahwan S, Lamantea E, Bizzi A, Bakhsh E, Moroni I, et al. *GJA12* mutations in children with recessive hypomyelinating leukoencephalopathy. Neurology 2006; 67: 273–9.

Bukauskas FF, Bukauskiene A, Bennett MVL, Verselis VK. Gating properties of gap junction channels assembled from connexin43 and connexin43 fused with green fluorescent protein. Biophys J 2001; 81: 137–52.

Bukauskas FF, Jordan K, Bukauskiene A, Bennett MVL, Lampe PD, Laird DW, et al. Clustering of connexin 43-enhanced green fluorescent protein gap junction channels and functional coupling in living cells. Proc Natl Acad Sci USA 2000; 97: 2556–61.

Cotrina ML, Lin JHC, Nedergaard M. Adhesive properties of connexin hemichannels. Glia 2008; 56: 1791–8.

Dahl E, Manthey D, Chen Y, Schwarz HJ, Chang YS, Lalley PA, et al. Molecular cloning and functional expression of mouse connexin-30, a gap junction gene highly expressed in adult brain and skin. J Biol Chem 1996; 271: 17903–10.

Dermietzel R, Traub O, Hwang TK, Beyer E, Bennett MVL, Spray DC, et al. Differential expression of three gap junction proteins in developing and mature brain tissues. Proc Natl Acad Sci USA 1989; 86: 10148–52.

Dobrowolski R, Sommershof A, Willecke K. Some oculodentodigital dysplasia-associated Cx43 mutations cause increased hemichannel activity in addition to deficient gap junction channels. J Membrane Biol 2007; 219: 9–17.

el-Fouly MH, Trosko JE, Chang C. Scrape-loading and dye transfer. A rapid and simple technique to study gap junctional intercellular communication. Exp Cell Res 1987; 168: 422–30.

Elias LAB, Wang DD, Kriegstein AR. Gap junction adhesion is necessary for radial migration in the neocortex. Nature 2007; 448: 901–7.

Fink JK. Hereditary spastic paraplegia. Curr Neurol Neurosci Rep 2006; 6: 65–76.

Garbern J, Cambi F, Shy M, Kamholz J. The molecular pathogenesis of Pelizaeus-Merzbacher disease. Arch Neurol 1999; 56: 1210–4.

Garbern JY. Pelizaeus-Merzbacher disease: genetic and cellular pathogenesis. Cell Mol Life Sci 2007; 64: 50–65.

Hansen JJ, Dürr A, Cournu-Rebeix I, Georgopoulos C, Ang D, Nielsen MN, et al. Hereditary spastic paraplegia SPG13 is associated with a mutation in the gene encoding the mitochondrial chaperonin Hsp60. Am J Hum Genet 2002; 70: 1328–32.

Henneke M, Combes P, Diekmann S, Bertini E, Brockmann K, Burlina AP, et al. *GJA12* mutations are a rare cause of Pelizaeus-Merzbacher-like disease. Neurology 2008; 70: 748–54.

Hudson LD, Garbern JY, Kamholz JA. Pelizaeus-Merzbacher disease. In: Lazzarini RA, editor. Myelin biology and disorders. Vol 2. San Diego: Elsevier; 2004. p. 867–85.

Inoue K. *PLP1*-related inherited dysmyelinating disorders: Pelizaeus-Merzbacher disease and spastic paraplegia type 2. Neurogenetics 2005; 6: 1–16.

Kamasawa N, Sik A, Morita M, Yasumura T, Davidson KGV, Nagy JI, et al. Connexin-47 and connexin-32 in gap junctions of oligodendrocyte somata, myelin sheaths, paranodal loops and Schmidt-Lanterman incisures: Implications for ionic homeostasis and potassium siphoning. Neuroscience 2005; 136: 65–86.

Kleopa KA, Orthmann JL, Enriquez A, Paul DL, Scherer SS. Unique distributions of the gap junction proteins connexin29, connexin32, and connexin47 in oligodendrocytes. Glia 2004; 47: 346–57.

Kumar NM, Gilula NB. The gap junction communication channel. Cell 1996; 84: 381–9.

Kunzelmann P, Schroder W, Traub O, Steinhauser C, Dermietzel R, Willecke K. Late onset and increasing expression of the gap junction protein connexin30 in adult murine brain and long-term cultured astrocytes. Glia 1999; 25: 111–9.

Lee ES, Moon HK, Park YH, Garbern J, Hobson GM. A case of complicated spastic paraplegia 2 due to a point mutation in the proteolipid protein 1 gene. J Neurol Sci 2004; 224: 83–7.

Li J, Hertzberg EL, Nagy JI. Connexin32 in oligodendrocytes and association with myelinated fibers in mouse and rat brain. J Comp Neurol 1997; 379: 571–91.

Li X, Ionescu AV, Lynn BD, Lu S, Kamasawa N, Morita M, et al. Connexin47, connexin29 and connexin32 co-expression in oligodendrocytes and Cx47 association with zonula occludens-1 (ZO-1) in mouse brain. Neuroscience 2004; 126: 611–30.

Li X, Lynn BD, Olson C, Meier C, Davidson KGV, Yasumura T, et al. Connexin29 expression, immunocytochemistry and freeze-fracture replica immunogold labelling (FRIL) in sciatic nerve. Eur J Neurosci 2002; 16: 795–806.

Magen D, Georgopoulos C, Bross P, Ang D, Segev Y, Goldsher D, et al. Mitochondrial Hsp60 chaperonopathy causes an autosomal-recessive neurodegenerative disorder linked to brain hypomyelination and leukodystrophy. Am J Hum Genet 2008; 83: 30–42.

Menichella DM, Goodenough DA, Sirkowski E, Scherer SS, Paul DL. Connexins are critical for normal myelination in the central nervous system. J Neurosci 2003; 23: 5963–73.

Menichella DM, Majdan M, Awatramani R, Goodenough DA, Sirkowski E, Scherer SS, et al. Genetic and physiological evidence that oligodendrocyte gap junctions contribute to spatial buffering of potassium released during neuronal activity. J Neurosci 2006; 26: 10984–91.

Micevych PE, Abelson L. Distribution of mRNAs coding for liver and heart gap junction proteins in the rat central nervous system. J Comp Neurol 1991; 305: 96–118.

Mugnaini E. Cell junctions of astrocytes, ependyma, and related cells in the mammalian central nervous system, with emphasis on the hypothesis of a generalized functional syncytium of supporting cells. In: Federoff S, Vernadakis A, editors. Astrocytes. Vol. 1. Orlando: Academic Press (Elsevier); 1986. p. 329–71.

Nagy JI, Ionescu AV, Lynn BD, Rash JE. Connexin29 and connexin32 at oligodendrocyte and astrocyte gap junctions and in myelin of the mouse central nervous system. J Comp Neurol 2003a; 464: 356–70.

Nagy JI, Ionescu AV, Lynn BD, Rash JE. Coupling of astrocyte connexins Cx26, Cx30, Cx43 to oligodendrocyte Cx29, Cx32, Cx47: implications from normal and connexin32 knockout mice. Glia 2003b; 44: 205–18.

Nagy JI, Li XB, Rempel J, Stelmack G, Patel D, Staines WA, et al. Connexin26 in adult rodent central nervous system: demonstration at astrocytic gap junctions and colocalization with connexin30 and connexin43. J Comp Neurol 2001; 441: 302–23.

Nagy JI, Ochalski PAY, Li J, Hertzberg EL. Evidence for the co-localization of another connexin with connexin-43 at astrocytic gap junctions in rat brain. Neuroscience 1997; 78: 533–48.

Nagy JI, Patel D, Ochalski PAY, Stelmack GL. Connexin30 in rodent, cat and human brain: selective expression in gray matter astrocytes, co-localization with connexin43 at gap junctions and late developmental appearance. Neuroscience 1999; 88: 447–68.

Nave K-A, Boespflug-Tanguy O. X-linked developmental defects of myelin formation: from mouse mutants to human genetic diseases. Neuroscientist 1996; 2: 33–43.

Nave KA, Sereda MW, Ehrenreich H. Mechanisms of disease: inherited demyelinating neuropathies - from basic to clinical research. Nat Clin Pract Neurol 2007; 3: 453–64.

Odermatt B, Wellershaus K, Wallraff A, Seifert G, Degen G, Euwens C, et al. Connexin 47 (Cx47)-deficient mice with enhanced green fluorescent protein reporter gene reveal predominant oligodendrocytic expression of Cx47 and display vacuolized myelin in the CNS. J Neurosci 2003; 23: 4549–59.

Oh S, Ri Y, Bennett MVL, Trexler EB, Verselis VK, Bargiello TA. Changes in permeability caused by connexin 32 mutations underlie X-linked Charcot-Marie-Tooth disease. Neuron 1997; 19: 927–38.

Orthmann-Murphy JL, Abrams CK, Scherer SS. Gap junctions couple astrocytes and oligodendrocytes. J Mol Neurosci 2008; 35: 101–16.

Orthmann-Murphy JL, Enriquez AD, Abrams CK, Scherer SS. Loss-of-function *GJA12/Connexin47* mutations cause Pelizaeus-Merzbacher-like disease. Mol Cell Neurosci 2007a; 34: 629–41.

Orthmann-Murphy JL, Freidin M, Fischer E, Scherer SS, Abrams CK. Two distinct heterotypic channels mediate gap junction coupling between astrocyte and oligodendrocyte connexins. J Neurosci 2007b; 27: 13949–57.

Prochnow N, Dermietzel R. Connexons and cell adhesion: a romantic phase. Histochemistry Cell Biol 2008; 130: 71–7.

Rash JE, Yasumura T, Dudek FE, Nagy JI. Cell-specific expression of connexins and evidence of restricted gap junctional coupling between glial cells and between neurons. J Neurosci 2001; 21: 1983–2000.

Richardson RR, Donnai D, Meire F, Dixon MJ. Expression of *Gja1* correlates with the phenotype observed in oculodentodigital syndrome/type III syndactyly. J Med Genet 2004; 41: 60–7.

Salviati L, Trevisson E, Baldoin MC, Toldo I, Sartori S, Calderone M, et al. A novel deletion in the *GJA12* gene causes Pelizaeus-Merzbacher-like disease. Neurogenetics 2007; 8: 57–60.

Scherer SS, Deschênes SM, Xu Y-T, Grinspan JB, Fischbeck KH, Paul DL. Connexin32 is a myelin-related protein in the PNS and CNS. J Neurosci 1995; 15: 8281–94.

Scherer SS, Wrabetz L. Molecular mechanisms of inherited demyelinating neuropathies. Glia 2008; 56: 1578–89.

Soher B, van Zijl P, Duyn J, Barker PB. Quantitative proton MR spectroscopic imaging of the human brain. Magn Reson Med 1996; 35: 356–63.

Swenson KI, Jordan JR, Beyer EC, Paul DL. Formation of gap junctions by expression of connexins in Xenopus oocyte pairs. Cell 1989; 57: 145–55.

Trosko JE, Change CC, Wilson MR, Upham B, Hayashi T, Wade M. Gap junctions and the regulation of cellular functions of stem cells during development and differentiation. Methods 2000; 20: 245–64.

Uhlenberg B, Schuelke M, Ruschendorf F, Ruf N, Kaindl AM, Henneke M, et al. Mutations in the gene encoding gap junction protein alpha 12 (connexin 46.6) cause Pelizaeus-Merzbacher-like disease. Amer J Hum Genet 2004; 75: 251–60.

Werner R, Levine E, Rabadan-Diehl C, Dahl G. Formation of hybrid cell-cell channels. Proc Natl Acad Sci USA 1989; 86: 5380–4.

Willecke K, Eiberger J, Degen J, Eckardt D, Romualdi A, Guldenagel M, et al. Structural and functional diversity of connexin genes in the mouse and human genome. Biol Chem 2002; 383: 725–37.

Wolf NI, Cundall M, Rutland P, Rosser E, Surtees R, Benton S, et al. Frameshift mutation in *GJA12* leading to nystagmus, spastic ataxia and CNS dys-/demyelination. Neurogenetics 2007; 8: 39–44.

Yamamoto T, Ochalski A, Hertzberg EL, Nagy JI. LM and EM immunolocalization of the gap junctional protein connexin 43 in rat brain. Brain Res 1990; 508: 313–9.

Yeager M, Nicholson BJ. Structure of gap junction intercellular channels. Curr Opin Struct Biol 1996; 6: 183–92.